Temporal and spatial dynamics of large lake hypoxia: Integrating statistical and three-dimensional dynamic models to enhance lake management criteria

Short (running) title: Large lake hypoxia: Integrating models to enhance lake management

Serghei A. Bocaniov[1, §, *] and Donald Scavia[1, £]

[1] Graham Sustainability Institute, University of Michigan, Ann Arbor, Michigan 48103, United States; [§] ORCID ID #: 0000-0001-5988-2034; [£] ORCID ID #: 0000-0002-2784-8269

* Correspondence to: S. A. Bocaniov, e-mail: bocaniov@umich.edu

Key Points:

- We modeled seasonal and spatial dynamics of low dissolved oxygen (DO) conditions (hypoxia) in central Lake Erie
- We showed hypoxia starts and can be extensive in the nearshore and can extend well beyond the time of traditional monitoring programs
- We recommend adjustments to monitoring programs and explore the impacts of using different DO thresholds defining hypoxia

Accepted Article

This is the author manuscript accepted for publication and has undergone full peer review but has not been through the copyediting, typesetting, pagination and proofreading process, which may lead to differences between this version and the Version record. Please cite this article as doi:10.1002/2015WR018170.

This article is protected by copyright. All rights reserved.

Abstract

Hypoxia or low bottom water dissolved oxygen (DO) is a world-wide problem of management concern requiring an understanding and ability to monitor and predict its spatial and temporal dynamics. However, this is often made difficult in large lakes and coastal oceans because of limited spatial and temporal coverage of field observations. We used a calibrated and validated three-dimensional ecological model of Lake Erie to extend a statistical relationship between hypoxic extent and bottom water DO concentrations to explore implications of the broader temporal and spatial development and dissipation of hypoxia.

We provide the first numerical demonstration that hypoxia initiates in the nearshore, not the deep portion of the basin, and that the threshold used to define hypoxia matters in both spatial and temporal dynamics and in its sensitivity to climate. We show that existing monitoring programs likely underestimate both maximum hypoxic extent and the importance of low oxygen in the nearshore, discuss implications for ecosystem and drinking water protection, and recommend how these results could be used to efficiently and economically extend monitoring programs.

Key words: Lake Erie, hypoxia, monitoring, modeling

Accepted Article

This article is protected by copyright. All rights reserved.

Introduction

Monitoring, modeling, and predicting areas of low dissolved oxygen (DO) in the Great Lakes and coastal oceans is important because the number and size of these regions have increased (Diaz, 2001; Diaz and Rosenberg, 2008; Vaquer-Sunyer and Duarte, 2008) and more management programs are being put in place to reduce them (e.g. *Lake Erie*: Hawley et al., 2006; IJC, 2012. *Gulf of Mexico*: MR/GOM, 2001, 2008. *Chesapeake Bay*: USEPA, 2010; CBWA, 2014. *Baltic Sea*: HELCOM, 2007. *Black Sea*: ICPDR, 2006, 2009). However, developing and testing models to guide management action, as well as tracking progress associated with those actions, are often hampered by financially constrained monitoring programs. For example, the Gulf of Mexico's hypoxic zone, the largest in the U.S.A. and the world's second-largest coastal hypoxic zone (Rabalais et al., 2007), is sampled systematically only once each year (Rabalais et al., 2002; Obenour et al., 2013). Similarly, estimates of Lake Erie's hypoxic area are generally based on only one or two sampling cruises (Zhou et al., 2013). Recent advances in geostatistical modeling have improved those estimates. For example, Obenour et al. (2015) used auxiliary spatial information to improve hypoxic area estimates with quantified uncertainties for the Gulf of Mexico, and Zhou et al. (2013, 2014, 2015) and Hansson et al. (2011) used similar methods to provide best estimates and uncertainties for Lake Erie, Chesapeake Bay, and the Baltic Sea. However improved, these snapshots in time still constrain analysis of both long-term and seasonal trends in hypoxia development because they often miss critical periods of development and dissipation and likely underestimate the maximum extent, a typical endpoint of management concern (MR/GOM, 2001, 2008; IJC, 2012). While additional monitoring can fill this gap, fiscal constraints have prohibited expanded monitoring as demonstrated by the lack of expanded monitoring efforts in many of these systems. Process-based, dynamic model interpolation of the sparse monitoring results can help provide important information. The aim of this study is to use

This article is protected by copyright. All rights reserved.

Accepted Article

a calibrated three-dimensional (3D) hydrodynamic-ecological model to expand a relationship developed by Zhou et al. (2013) to estimate Lake Erie's hypoxic area (DO < 2 mg L^{-1}) as a function of average bottom water DO concentration from 10 central basin index stations. In doing so, we can explore the temporal and spatial development and dissipation of low-oxygen conditions in Lake Erie.

Lake Erie supports a multi-billion dollar fishery and serves more than 11 million people in the United States and Canada. It experienced cultural eutrophication (Beeton, 1963), recovery in response to nutrient load reductions (DePinto et al., 1986), and a recent return to eutrophic conditions (Burns et al., 2005; Bridgeman et al., 2013; Zhou et al., 2013; Michalak et al., 2013; Scavia et al., 2014), with phosphorus (P) loading (Dolan, 1993; Dolan and Chapra, 2012) being the key driver of all three phases. This re-eutrophication has resulted in hypoxic extents comparable to levels of the past, with some reaching over 10,000 km^2 (Zhou et al., 2013), which in some years are comparable to or exceeding that of Gulf of Mexico (Obenour et al., 2013).

The most common index used in monitoring, modeling, forecasting, and tracking hypoxia is the maximum areal extent of DO concentrations below 2 mg L^{-1} (Vaquer-Sunyer and Duarte, 2008). The work described herein is an effort to explore three aspects of that index: *thresholds, location, and dynamics.*

Thresholds – Though hypoxia can be defined as DO concentrations below 5-6 mg L^{-1} in freshwater and below 2-3 mg L^{-1} in marine and estuarine systems (Farrell and Richards, 2009), there is a broad range of definitions ranging from about 0.3 to 4 mg L^{-1} with an overall mean of 2.3 (Vaquer-Sunuer and Duarte, 2008: $N = 49$ studies). The most commonly used index is 2 mg L^{-1} (e.g. CENR, 2000; Diaz, 2001; Zhou et al., 2013, 2014, 2015; Rucinski et al., 2014), the point below which most aquatic organisms start to suffocate (Diaz, 2001), first suggested by Renaud

This article is protected by copyright. All rights reserved.

(1986) based on the observations of fisheries collapse in Louisiana coastal waters. However, both higher and lower DO concentrations have negative ecosystem effects (Vaquer-Sunuer and Duarte, 2008). For example (see Tables S1 and S2 in Supporting Information - SI), DO < 1 mg L^{-1} causes substantial mortality in juvenile fish, DO < 3 mg L^{-1} forces Lake Erie fishes to migrate to areas with higher concentrations, DO < 4 mg L^{-1} is an acute mortality limit for invertebrates, and DO < 5 mg L^{-1} is a general suboptimal concentration for fish.

Location and dynamics – The location and dynamics (timing, frequency, and duration) of hypoxia can affect the growth, distribution, and mortality of sessile and mobile aquatic organisms, including fishes of high economic importance (Arend et al., 2011). Location is important because hypoxia can spatially overlap with otherwise high quality habitats and/or ecologically important literal zones, limiting access to the areas of desirable thermal and light conditions, and/or habitats suitable for foraging, spawning, nursing or protection from predation (Roberts et al., 2009; Vanderploeg et al., 2009; Rao et al., 2014; Kraus et al., 2015). Timing is also important because hypoxia can occur during critical periods of spawning, egg development, and other recruitment stages (Arend et al., 2011).

Unlike its coastal marine counterparts, Lake Erie is also an important drinking water source. Water withdrawals from nearshore intakes can be as high as 68.9 km^3 $year^{-1}$ (2011 data; GLC, 2013) representing 14.2 % of the entire lake volume. Hypoxic and anoxic waters have low pH (e.g. Howarth et al., 2011) and elevated concentrations of manganese (Mn; e.g. Davison, 1993) and other contaminants mobilized from the sediments. When such waters enter the distribution system, they compromise the water supply through enhanced pipeline and equipment corrosion; staining of fixtures, equipment, swimming pools, and laundry (Sly et al., 1990); and often results in undesirable color of tap water. A strategy is emerging to use a buoy-based

This article is protected by copyright. All rights reserved.

monitoring system near water intakes to alert shutdowns at the appearance of the advected anoxic water (Ruberg et al., 2008; CENR, 2010). For example, the National Oceanic and Atmospheric Administration (NOAA) and the Cleveland Water Department deployed a buoy-based hypoxia early warning system that employs sensors near the water intakes to provide advance warning of hypoxia after three of four Cleveland water treatment plants were exposed to anoxic water in 2006, compromising the safety of the water supply for 1.5 million people (Ruberg et al., 2008). While promising, the effectiveness of such strategies may be limited when more advance warning or prediction is needed to prepare for altered treatment strategies. Because water intakes are generally located in the nearshore zone, it could be important to better characterize the seasonal dynamics and inter-annual variability of nearshore hypoxia and anoxia.

Methods

Study site description – Lake Erie is located in North America (41°00'N - 43°00'N latitude, 78°50'W - 83°50'W longitude), and has three distinct basins, west, central, and east (Fig. 1). Its central basin is approximately 63% of both total lake surface and volume (Bolsenga and Herdendorf, 1993). Its surface area and volume are 16,138 km^2 and 305 km^3, and mean and maximum depths are 18.3 and 25.6 m. Depth-specific surface area and volume show maxima at depths of 20 and 22 m. Using the 20 m contour as a boundary, the nearshore (≤ 20 m) zone represent approximately 62.5% of central basin area and 53.4% of central basin volume.

Statistical Model - Zhou et al. (2013) provided a useful statistical relationship between hypoxic area and the average bottom water DO concentration from ten Lake Erie index stations (Table 1) visited routinely by the United States Environmentally Protection Agency (USEPA):

$$HE_2 = a \cdot e^{\left(\frac{-DO_m^2}{b}\right)} \qquad \text{(Equation 1)}$$

This article is protected by copyright. All rights reserved.

where HE_2 is the area (10^3 km^2) with DO < 2 mg L^{-1}, DO_m is the mean DO concentration across the ten USEPA index stations (Table 1), *a* and *b* equal 9.30 and 7.09, respectively (Zhou et al., 2013; $R^2 = 0.97$, $N = 75$ cruises). We use the form of Equation 1 throughout our analysis.

3D Modeling – Our ecological model is based on the dynamically coupled hydrodynamic-biogeochemical models, ELCOM-CAEDYM (ELCD). The Estuary and Lake Computer Model (ELCOM) is a three-dimensional hydrodynamic model that dynamically simulates water levels, thermal structure, temperature, velocity, and salinity distributions (Hodges et al., 2000; Hodges and Dallimore, 2006). ELCOM is dynamically coupled with the Computational Aquatic Ecosystem Dynamics Model (CAEDYM; Hipsey, 2008), a bio-geochemical model capable of simulating of many biological, chemical, and sediment processes, as well as macrophytes, invasive species such as *Dreissenid* mussels (Bocaniov et al., 2014a) and several phytoplankton functional groups.

The ELCD model configuration was set similar to its previous applications to Lake Erie (e.g. Bocaniov et al., 2014a). Lake Erie bathymetry was obtained from the NOAA National Geophysical Data Center. The physical domain was discretized into 2 x 2 km surface grids with 45 unevenly spaced vertical layers (0.5 to 5 m) to create the 3D Cartesian mesh for the computational domain. Within the central basin, vertical layers were between 0.5 and 1 m thick. The time step was 300 s with output recorded every hour for water quality profiles and every 2 hours for the bottom and surface layers. The model was run for 191 days from April 21, 2008 (DOY 112), the first date with sufficient initial conditions from the USEPA cruises, to October 28, 2008 (DOY 302), a date soon after the lake becomes well mixed and hypoxia dissipates.

In-lake initial conditions (water temperature, chemistry, and biology) were based on data from the USEPA Great Lakes National Program Office (GLNPO) monitoring program, derived

This article is protected by copyright. All rights reserved.

from observations at twenty stations (Fig. 1; east basin: ER9, ER10, ER15, ER63; central basin: ER30, ER31, ER32, ER36, ER37, ER38, ER42, ER43, ER73, ER78; west basin: ER58, ER59, ER60, ER61, ER91, ER92). These data were downloaded from the Great Lakes Environmental Database (GLENDA) available on the EPA Central Data Exchange (CDX) website [Web. 11 May. 2015. <https://cdx.epa.gov/epa_home.asp>].

To account for spatial variability in meteorological drivers across such a large lake, meteorological forcing was represented by 13 different but approximately equal-sized zones (Fig. S1, see Supporting Information - SI). Hourly meteorological observations of air temperature, wind speed, wind direction, relative humidity, solar radiation (shortwave), and cloud cover at 21 coastal stations and three in-lake buoys operated by the National Data Buoy Center and Environment Canada were corrected to account for the differences between over-land and over-lake conditions based on empirical relationships developed for Lake Erie (Rodgers and Anderson, 1961; Schwab and Morton, 1984; Schertzer, 1987), and then spatially interpolated to the 13 zones using a method of Sambridge et al. (1995). Incoming longwave radiation was calculated first for the clear sky conditions (Idso and Jackson, 1969) and then adjusted for cloud cover (Parkinson and Washington, 1979).

One major outflow (Niagara River) and the nineteen tributaries responsible for the majority of the discharge and nutrient loads to the lake (Table 2) were represented in the model (Fig. 1). Four tributaries enter the west basin, eleven to the central basin, and four to the east basin. Concentrations of the water quality constituents, daily flow rates, and water temperatures for all tributaries were gathered from the Michigan Department of Environmental Quality (MDEQ), Heidelberg University Water Quality Laboratory, United States Geological Survey (USGS), Great Lakes Environmental Research Laboratory's (GLERL), STORET database of

This article is protected by copyright. All rights reserved.

Accepted Article

USEPA, Water Survey of Canada (Environment Canada), Provincial Water Quality Monitoring Network (PWQMN; Ontario, Canada) and Grand River Conservation Authorities (GRCA; Ontario, Canada).

Our main objective was to develop predictive equations for hypoxic extent that can be valid over the wide range of the meteorological conditions. To accomplish that, we used meteorological drivers representing the 'warmest', 'coldest' and 'normal' years derived from the observed historical record of lake-wide surface water temperature. Daily lake-wide average surface water temperatures for 1995 to 2014, derived from the remote-sensing observations, were downloaded from Great Lakes Surface Environmental Analysis (GLSEA) website [Web. 11 May. 2015. <http://coastwatch.glerl.noaa.gov/statistic/statistic.html>]. To determine baseline average conditions for this period, average daily mean lake surface temperatures were calculated for each day of the year by averaging all available data for each day over that 20 year period. The Root Mean Squared Error (RMSE) and Percent Bias (PBIAS) were calculated (Table S3, SI) for each year relative to the baseline conditions. The RMSE was calculated separately for the entire year, as well as for the open water season (April 1 to October 30). The 'normal' year was defined as the year with the smallest RMSE and PBIAS (2008; see below). PBIAS was used to determine both the warmest year (the largest absolute value of negative PBIAS; 2012, see below) and 'coldest' year (the largest positive value of PBIAS; 1996, see below). Our baseline scenario used initial and boundary conditions from the 'normal' meteorological year. 'Warm' and 'cool' scenarios used initial conditions, inflows/outflows, and nutrient load unchanged from the 'normal' year, and meteorological conditions corresponding to those scenario years.

We use nutrient loads across all cases comparable to the current Lake Erie target load of 11,000 metric tonnes per annum (MTA) for all scenarios, determined by selecting loads from the

This article is protected by copyright. All rights reserved.

Accepted Article

year with the smallest absolute percent difference from the target load. This analysis identified both 1996 and 2008 but because 1996 lacked sufficient field observations for model validation, we used 2008.

In an earlier application to Lake Erie, ELCD was calibrated for 2002 for several of the most important water quality variables (major nutrients and their fractions; total phytoplankton biomass; light attenuation; suspended solids) and the seasonal succession of the major phytoplankton taxonomic groups (Leon et al., 2011). In later applications for the same calibration year, it was extended to investigate mussels' role in the decline of Lake Erie's phytoplankton spring blooms (Bocaniov et al., 2014a). The model was also previously validated for water temperature and thermal structure for 2008 (Liu et al., 2014). Herein, we used the same calibration and extended that validation for DO and temperature at several spatial scales using a similar model configuration, but with higher resolution of meteorological input (13 vs. 4 zones) and increased number of the tributaries (19 vs. 11). In addition to the earlier validation work, the model's ability to reproduce the most dynamic part of the thermal structure (metalimnion) was analyzed quantitatively by comparing observed and modeled width and depth (thermocline position). The depth of the thermocline and the upper and lower boundaries of the metalimnion were determined with a fitting approach similar to that of Read et al. (2011) using the observed and modelled temperature profiles which were converted to the density profiles. Data for validation came from water quality profiles measured in the central basin by USEPA during seven cruises in 2008 (April 20-22, June 2-3; June 24-25; July 12-13; August 10-11; August 30-31; and, September 12-13). Validation data for the satellite-based lake-wide surface temperature observations in 2008 were obtained from the GLSEA website [Web. 12 May. 2015. <http://coastwatch.glerl.noaa.gov/statistic/statistic.html>].

This article is protected by copyright. All rights reserved.

Accepted Article

3D model-derived relationships between low DO areas and bottom DO – To derive predictive equations for low DO areas (HE_i; HE is the hypoxic extent and *i* is the DO threshold concentration being evaluated), we ran the model for the 'normal' year and calculated the daily areal extent of the hypoxic area based on 2 different thresholds (HE_2 , DO < 2 mg L^{-1}; HE_1, DO < 1 mg L^{-1}) and the mean daily simulated bottom DO concentrations at the locations of the USEPA and the Environment Canada index central basin stations (Table 1). Using the curve-fitting function in R (R Core Team, 2014), we fit Equation 1 to determine parameters *a* and *b* and their 95% confidence intervals (Table 3). We then used a similar approach using a pooled data set consisting of the simulation results for the 'normal', 'cool', and 'warm' years to derive the predictive equations for all 4 thresholds, HE_1, HE_2, HE_3 (DO < 3 mg L^{-1}), and HE_4 (DO < 4 mg L^{-1}).

Seasonal trend in stratification, thermal stability, and potential for mixing - To investigate the seasonal patterns in stratification and wind fields we computed the basin-wide daily surface (depth ≤ 0.5 m) and bottom (depth > 20 m) temperatures (T_s and T_b) and wind speed. To quantify the importance of water column stability (thermal stratification) we calculated the Schmidt stability (*S*; Schmidt, 1928; Idso, 1973), Brunt-Väisälä frequency (N^2; Väisälä, 1925; Brunt, 1927), and wind stress (τ; Imberger, 1985). The time series of daily values of τ, *S* and N^2 were computed for the conditions at station ER78 (Fig. 1) using observed wind speed and simulated temperature profile assumed to be a good representation of the typical profile of stratification in the central basin.

Results

This article is protected by copyright. All rights reserved.

Our ELCD validation demonstrates the model's ability to adequately represent the 2008 field observations. The agreement between the observed and simulated temperatures was good, particularly for the lake wide surface temperature (Fig. 2a, b; RMSE = 0.8°C, N = 191) and in the top six meters of the surface mixed layer (Fig. 2c; RMSE = 1.17°C, N = 70) which is good representative of the epilimnetic conditions in central Lake Erie (Leon et al., 2011; Bocaniov et al., 2014a). Simulated bottom temperature at the ten index USEPA stations that are representative of the central basin (Table 1) was also in good agreement with observations for all cruises (Fig. 2d; RMSE = 1.99°C, N = 70) and the thermal structure of the central basin was well represented (Fig. 3a-n). The calculated RMSE between the measured and simulated profiles for stations ER31 (Fig 3a-g) and ER78 (Fig 3h-n), with comparisons made at 0.5 m depth increments, were 1.46°C (N = 280) and 1.95°C (N = 280), respectively. Simulated temperatures in the epilimnion and at the lower metalimnetic boundaries were in good agreement with the observed profiles (Fig. 3a-n). Simulated temperatures in the hypolimnion agreed within 1 or 2°C with the observed temperatures (Fig 3a-n). The modeled thermocline position was reproduced well by model (Table S4, SI). The width of the simulated metalimnion was wider than observed but the differences between the mean simulated and observed boundaries were smaller than the standard deviation of both observations and model for a given boundary. On average, the model had a small tendency to underestimate the depth of the upper metalimnetic boundary (PBIAS = 14.6%; N = 50) and overestimate the depth of the lower boundary (PBIAS = -8.5%; N = 50). Simulated DO concentrations were in good agreement with the observed values in the water column (Fig. 3o-r; RMSE = 1.22 mg L^{-1}, N = 149) and at the lake bottom (Fig. 4a-d; RMSE = 1.16 mg L^{-1}, N = 70). The regression analysis (major axis model II regression, Fig. 4e) showed that the slope and the intercept were not significantly different from one and zero. The t-test also

This article is protected by copyright. All rights reserved.

Accepted Article

indicated no significant difference between observed and simulated mean bottom DO (t = 1.7504, df = 69, P = 0.085).

Lake thermal structure, water column stability and potential for wind-induced mixing - The seasonal dynamics of the surface temperatures (T_s) in the central basin followed the seasonal cycle of solar radiation (Fig. S2a, SI), increasing in spring and early summer, peaking from mid-July to early August, and declining afterwards. Bottom temperature (T_b) steadily increased during the stratification period with a somewhat higher rate of increase near the end of the period (Fig. S2a, SI). The difference between T_s and T_b was small in April (22 April 2008: 1.7 °C) but increased over the warming season, approached its maximum values in July (12.0 °C), and declined to zero at lake overturn in early October (Fig. S2a, SI).

Overall, the temporal dynamic of winds over the lake surface also exhibited a clear seasonal pattern (Fig. S2a, SI). Winds were higher in the spring (April through May), weaker in early and mid-summer (June and July) and stronger in August and September, with the strongest winds in October. Winds were variable and episodic with weaker and stronger episodes with strong wind events typically occurring at 7 to 10 day intervals (Fig. S2a, SI). The computed values for Schmidt (S) and water column (N^2) stability showed seasonal patterns similar to observed T_s, mimicking the lake seasonal heating cycle (Fig. S2, SI). Water column stability and its resistance to wind mixing as judged by S and N^2 were low in spring but then increased rapidly from late May through June, reaching the seasonal maximum in July, and diminishing afterwards. The strong wind events and corresponding high wind stress had noticeable effects on the lake thermal stability with increasing influences during the cooling phase and subsequent decline in the strength of thermal stability (August through September; Fig. S2b, SI).

This article is protected by copyright. All rights reserved.

Accepted Article

Estimating Hypoxic Extent from index stations - There was good correspondence between simulated daily hypoxic extent (HE_2) for the baseline scenario and estimates using Equation 1 (Zhou et al., 2013; herein referred to as the Zhou model) and mean simulated daily bottom DO concentrations (DO_m; mg L^{-1}) at the locations of ten USEPA index stations (Table 1; Fig. 5a) until mid-September (Fig. 5a-b). However, simulated mid-September to late October results often diverged from those predicted by the Zhou model (Fig. 5a, c). Comparison of simulated hypoxic extent with estimates derived from the Zhou model and DO_m from simulated and field bottom DO concentrations at index stations showed good agreement overall, although the results derived from the Zhou model for early and mid-autumn again tend to underestimate the simulated results (Fig. 5d; sim 1 vs. sim 2).

The comparison of simulated hypoxic extent HE_2 (Table 4) using Equation 3 from Table 3 and observed field data for the GLNPO cruises from 2000 to 2012 with those reported by Zhou et al. (2013, 2015) was also very good (Fig. 6a). A regression analysis (major axis model II regression, $N = 18$, $P < 0.01$) comparing the two estimates revealed that the slope was not significantly different from 1 (slope = 0.98 [95% CI: 0.89; 1.08] and while the intercept was significantly different from zero (intercept = 0.83 [95% CI: 0.43; 1.19]), it was small, indicating a small systematic difference (0.83×10^3 km^2) between the two estimates. Nevertheless, all predicted values by Equation 3 from Table 3 were within the range of the 95% C.I. reported by Zhou et al. (2013, 2015). A one to one comparison of the results for selected cruises in 2003, 2005, and 2012 also revealed a reasonable match between the predictions of HE_2 using Equation 3 and those calculated from the geostatistical method (Zhou et al., 2013, 2014) (Fig. 6b).

Estimating anoxic area - Simulated daily HE_1 extent (DO < 1 mg L^{-1}; called anoxic extent herein) as a function of simulated mean daily DO concentrations (DO_m) at the USEPA

This article is protected by copyright. All rights reserved.

Accepted Article

index stations (Table 1) followed a pattern similar to that for HE_2 (Fig. 7a) with additional outliers during a six-day strong wind event (August 26-31, 2008; Fig. S2, SI) that indicate a potentially higher sensitivity of HE_1 compared to HE_2 to wind events. When periods corresponding to the strong winds (August 26-31, 2008) and early mid-autumn (September 14 to October 28, 2008) were excluded, the relationship between HE_1 and DO_m was very strong (R^2 = 0.97; Fig. 7b). The analysis also revealed a non-linear relationship between HE_1 and HE_2 (Fig. 7c). Comparison between the model simulations of the HE_1 with those predicted from the simulated daily DO_m using an equation shown in Fig. 7b demonstrates a very good fit between two compared datasets (Fig. 7d) and confidence in using the bottom DO concentrations at the ten USEPA index stations in the central basin to estimate the spatial extent of both HE_1 and HE_2.

Estimating HE_1, HE_2, HE_3, and HE_4 for a wider range of meteorological conditions - Using the approach outlined above, we developed predictive equations for simulated HE_1, HE_2, HE_3 and HE_4 as a function of mean bottom DO concentrations observed at either the USEPA index stations or Environment Canada index stations (Table 1) for the pooled dataset representing 'normal', 'cool', and 'warm' years. The resulting equations have high R^2 values (Table 3), indicating good fit overall. Using Equations 2-5 (Table 3) we calculated the HE_1, HE_2, HE_3 and HE_4 using average measured concentrations from the August USEPA cruises in 2000 through 2014 (Fig. 8). Results show that areal extents for lower DO thresholds have larger inter-annual variability. For example, the average absolute percent difference between annual values and their overall (inter-annual) mean were 119%, 78%, 57% and 37% for HE_1, HE_2, HE_3 and HE_4, respectively.

Spatial seasonal dynamics of total, nearshore, and offshore hypoxia – Simulated seasonal dynamics of HE_1 and HE_2 are compared for the entire central basin, as well as separately for the

This article is protected by copyright. All rights reserved.

Accepted Article

nearshore and offshore zones, for 'normal' (Fig. 9a-b), 'cool' (Fig. 9c-d), and 'warm' (Fig. 9e-f) years. As expected, whole-basin HE_2 was larger during the 'warm' year and smaller during the 'cool' year compared to the 'normal' year. Anoxia (HE_1) was also the smallest during the 'cool' year but somewhat larger in the 'normal' year compared to the 'warm' year (Fig. 9a, c, e). Results also show that HE_2 starts first in the nearshore and then extends further to the offshore (Fig. 9b, d, f). A similar pattern was observed with HE_1 (Fig. 9a, c, e) although it was not as clear for the 'normal' year (Fig. 9a). Nearshore HE_1 and HE_2 were nearly the same offshore in 'cool' and 'warm' years, but smaller in the 'normal' year (Fig. 9a-f).

Comparing seasonal dynamics of HE_1, HE_2, HE_3, and HE_4 for 'normal' (Fig. 10a), 'cool' (Fig. 10b) and 'warm' (Fig. 10c) years showed that HE_3 and HE_4 appear less affected by the warm and cool extremes from the historical record, suggesting that their timing and extent are more predictable under future climates (maximum extent: HE_3 = 10-12 x 10^3, and HE_4 = 12-13 x 10^3 km^2) compared to the lower thresholds. Also worth noting is that HE_3 and HE_4 can occupy the large proportions of the central basin for extended time periods.

Discussion

Model validation – We demonstrate the ability of ELCD, previously calibrated for 2002, to reproduce field observations from 2008 of average lake-wide surface temperatures (Fig. 2a-b), epilimnetic temperatures averaged over the top 6 m (Fig. 2c), bottom temperatures (Fig. 2d), thermal structure (Fig. 3a-n; Table S4, SI), and both surface and bottom DO concentrations (Figs. 3o-r & 4). The calculated RMSE were similar and within the range of those reported in other three-dimensional modeling studies (Huang et al., 2010; Leon et al., 2011; Beletsky et al., 2013; Liu et al., 2014; Bocaniov et al., 2014a, b). Accurately modeling Lake Erie's metalimnion

This article is protected by copyright. All rights reserved.

Accepted Article

dynamics is difficult due to numerical diffusion, a very sharp metalimnion (Schertzer et al., 1987), and its highly dynamic nature and sensitivity to wind fields (Beletsky et al., 2013). In addition, when present, it is the most dynamic part of the thermal structure so that small mismatches in time and space between modeled and observed phases appear as large errors. We are not aware of any other modeling studies of Lake Erie that quantitatively characterized the vertical structure of the modeled metalimnion (thermocline position, and upper and lower boundaries). Our results are a first attempt to do that, and we showed good comparisons to the thermocline depth (Table S4, SI) with upper and lower boundaries of the metalimnion represented reasonably well compared to the other Lake Erie studies (Beletsky et al., 2013; Liu et al., 2014). The more diffused nature of the modeled metalimnion in our study does not affect our results because the surface and bottom temperatures, the thermocline position (depth of the maximum change in density), and near-bottom oxygen dynamics are all well reproduced by model.

Seasonal Dynamics - Geostatistical modeling have improved estimates of the spatial extent of hypoxia in Lake Erie (Zhou et al., 2013, 2015); however, even these improved estimates are limited to relatively few snapshots in time constrained by the observation set. As a result, the regression model derived from those geostatistical estimates is limited to observations collected during basin-wide cruises through August or the first half of September (see Table S1 in Zhou et al., 2013), a period when stratification is still strong (e.g. Fig. S2b, SI) and hypoxic area may still be growing (Fig. 9; see also Fig. S2, SI). For example, the maximum possible hypoxic area derived from Zhou model is 9,300 km^2, whereas hypoxic area has been reported to be as large as 11,000 km^2 (Beeton, 1963; Table S1 in Zhou et al., 2013). This has important implications because several recent modeling efforts have used this relationship to convert zero-,

This article is protected by copyright. All rights reserved.

1- and 2-dimensional model outputs to hypoxic area (Scavia and DePinto, 2015) and the upper limit of the regression model may underestimate the ultimate hypoxic area later in the summer and fall. Because our results are consistent with Zhou et al. (2013) through August and early September, we were able to extend the application later in the year using equations derived from our ELCD model output. We also developed equations to estimate the hypoxic extents of different DO thresholds (1, 2, 3 and 4 mg L^{-1}) as a function of mean bottom DO at the locations of Environment Canada index stations (Table 1), in addition to the USEPA index station, so that Environment Canada data can also be used in estimates of hypoxic extent.

While our results agreed well with those predicted by Zhou model for the data through approximately mid-September (Fig. 5b), the divergence after that time (Fig. 5c, a) coincides with the beginning of lake destratification and appears to be a result of wind stress beginning to dominate buoyancy forces, implying different underlying processes are in play.

During much of the warming season, buoyancy force is sufficient to overcome mixing and prevent oxygen flux from the epilimnion, favoring hypoxia formation and stability (Fig. S2b, SI). During this period, hypoxic area can be predicted well from knowledge of bathymetry and DO concentrations at index stations (e.g. Zhou et al., 2013) because hypoxia development follows the bathymetry. However, when buoyancy forces decline in autumn (Fig. S2b, SI), hypoxia becomes more susceptible to strong wind events and associated mixing. At this time, the epilimnion deepens and the thermocline erodes as the lake continues to cool. As a result, Zhou's model may significantly underestimate hypoxic area at this time of year (Fig. 5c). In mid-autumn, as the thermocline erodes, episodes of high winds (Fig. S2, SI) become more important for short-term fluctuations in hypoxic extent (Fig. 5c; large variations and departures from 1:1

This article is protected by copyright. All rights reserved.

line), whereas the buoyancy is more important for longer time scales (e.g. Fig. 5b; points are getting closer to the 1:1 line).

Our results also demonstrate that hypoxic extent usually reaches its maximum in September (Fig. 9), whereas current monitoring programs typically end prior to that time. If maximum extent is a management metric (e.g. IJC, 2012), this suggests the need to add monitoring cruises through September, perhaps using models to schedule those later cruises adaptively. An alternative could be to deploy moorings with the DO sensors at 0.5 to 1 m above bottom at the locations of the USEPA index stations and use those observations and the equations in Table 3 to provide a more complete temporal characterization of seasonal hypoxia.

Different thresholds – Because the impacts of low DO concentrations differs among processes and organisms (Vaquer-Sunyer and Duarte, 2008; Farrell and Richards, 2009; Roberts et al., 2009; Vanderploeg et al., 2009; Tables S1 and S2, SI), we explored the dynamics of low oxygen areas defined by different thresholds. Our results (Fig. 10a-c) show that areas with DO less than 3 or 4 mg L^{-1} can occupy up to 75% and 85% of the central basin, respectively, and can last for as long as three months (e.g. Fig. 10c). Therefore, the commonly used DO threshold of 2 mg L^{-1} may fail to reflect conditions where aquatic organisms experience hypoxia-induced responses. Because these thresholds are likely species and process specific, it could be possible to set different targets for Lake Erie, and use the equations in Table 3 and data from the USEPA or EC index stations to track associated conditions.

Spatial dynamics - Despite a wide-spread belief that Lake Erie hypoxia starts at the deepest parts of the basin, our results present a first numerical demonstration that both hypoxia and anoxia start in the nearshore (Fig. 9). This may not be as clear during the 'normal' year simulations (Fig. 9a, b) but a closer examination shows that, even in that case, hypoxia appears

This article is protected by copyright. All rights reserved.

first in the nearshore *albeit* for only a short time. Current monitoring programs are usually aimed at offshore conditions. However, the nearshore zone (defined here as depths ≤ 20 m), occupies a very significant portion of surface area of the central basin, and is the location of important habitat and drinking water intakes that have to be protected from hypoxic and anoxic waters. Our findings also demonstrated that nearshore hypoxia is significant and exists for extended periods (Fig. 9), and that variations in climate, especially warmer meteorological conditions, may result in significant increases in hypoxia extent and duration in the nearshore (Fig. 9b, d, f). Therefore, it would be important to incorporate specific nearshore management criteria in future management and monitoring activities. In fact, the revised Great Lakes Water Quality Agreement (IJC, 2012) includes a new focus on the nearshore. It might be useful to employ the three-dimensional model like the one used here to identify critical areas in the nearshore for enhanced monitoring.

Acknowledgements

This work was supported in part by the National Science Foundation (NSF) under grant 1039043, the USEPA under contract EP-R5-11-07, Task Order 21, and the Graham Sustainability Institute of the University of Michigan. We are grateful to David Schwab for his advice and help with the interpolation of the meteorological data, as well as three anonymous reviewers. Data sets are available upon request by contacting the corresponding author (Serghei A. Bocaniov, bocaniov@umich.edu).

References

Arend, K. K., D. Beletsky, J. V. DePinto, S. A. Ludsin, J. J. Roberts, D. K. Rucinski, ... , and T. O. Höök (2011), Seasonal and interannual effects of hypoxia on fish habitat quality in central Lake Erie, *Freshwater Biol.*, 56(2), 366-383.

This article is protected by copyright. All rights reserved.

Beeton, A. M. (1963), Eutrophication of the St. Lawrence Great Lakes, *Limnol. Oceanogr*.,10, 240–254.

Beletsky, D., N. Hawley, and Y. R. Rao (2013), Modeling summer circulation and thermal structure of Lake Erie, *J. Geophys. Res. Oceans*, 118, 6238–6252.

Bocaniov, S. A., R. E. H. Smith, C. M. Spillman, M. R. Hipsey, and L. F. Leon (2014a), The nearshore shunt and the decline of the phytoplankton spring bloom in the Laurentian Great Lakes: Insights from a three-dimensional lake model, *Hydrobiologia*, 731, 151–172.

Bocaniov, S. A., C. Ullmann, K. Rinke, K. G. Lamb, and B. Boehrer (2014b), Internal waves and mixing in a stratified reservoir: insights from three-dimensional modeling, *Limnologica*, 49, 52-67.

Bolsenga, S., and C. Herdendorf (Eds.) (1993), Lake Erie and Lake St. Clair handbook. Wayne State University Press.

Bridgeman, T. B., J. D Chaffin, and J. F. Filbrun (2013), A novel method for tracking western Lake Erie Microcystis blooms, 2002–2011, *J. Great Lakes Res*., 39(1): 83-89.

Brunt, D. (1927), The period of simple vertical oscillations in the atmosphere, *Quart*. *J*. *Roy*. *Meteorol*. *Soc*., 53, 30-32.

Burns, N. M., D. C. Rockwell, P. E. Bertram, D. M. Dolan, and J. J. H. Ciborowski (2005), Trends in temperature, Secchi depth, and dissolved oxygen depletion rates in the central basin of Lake Erie, 1983–2002, *J. Great Lakes Res*., 31, 35–49.

CBWA (Chesapeake Bay Watershed Agreement) (2014), Chesapeake Bay Watershed Agreement. Chesapeake Bay Program. [Available at: <http://www.chesapeakebay.net/chesapeakebaywatershedagreement/page>; accessed 23 Jun 2015].

CENR (Committee on Environment and Natural Resources) (2010), Scientific assessment of hypoxia in U.S. coastal waters. Interagency Working Group on Harmful Algal Blooms, Hypoxia, and Human Health of the Joint Subcommittee on Ocean Science and Technology. Washington, DC. [Available at: <https://www.whitehouse.gov/sites/default/files/microsites/ostp/hypoxia-report.pdf>; accessed 23 Jun 2015].

This article is protected by copyright. All rights reserved.

Accepted Article

CENR (Committee on Environment and Natural Resources) (2000), An integrated assessment of hypoxia in the Northern Gulf of Mexico. National Science and Technology Council Committee on Environment and Natural Resources, Washington, DC., 58 pp. [Available at: <http://oceanservice.noaa.gov/products/hypox_finalfront.pdf>; accessed 23 Jun 2015].

Davison, W. (1993), Iron and manganese in lakes, *Earth Sci. Rev.,* 34(2), 119-163.

De Pinto, J. V., T. C Young, and L. M. McIlroy (1986), Great Lakes water quality improvement, *Environ. Sci. Technol.*, 20(8), 752-759.

Diaz, R. J. (2001), Overview of hypoxia around the world, *J. Environ. Qual*., 30(2), 275-281.

Diaz, R. J., and R. Rosenberg (2008), Spreading dead zones and consequences for marine ecosystems, *Science*, 321(5891), 926-929.

Dolan, D. M. (1993), Point source loadings of phosphorus to Lake Erie: 1986–1990, *J. Great Lakes Res*., 19(2), 212-223.

Dolan, D. M., and S. C. Chapra (2012), Great Lakes total phosphorus revisited: 1. Loading analysis and update (1994–2008), *J. Great Lakes Res*., 38(4), 730-740.

Farrell, A. P., and J. G. Richards (2009), Defining hypoxia: an integrative synthesis of the responses of fish to hypoxia. In: Richards JG, Farrell AP, Brauner CJ (eds) Hypoxia. Academic Press, London, pp 487–503, doi:10.1016/S1546-5098(08)00011-3.

GLC (Great Lakes Commission) (2013), Annual Report of the Great Lakes Regional water use database representing 2011 water use data. May 2013, Issue No. 21. [Available at: <http://projects.glc.org/waterusedata//pdf/wateruserpt2013.pdf>; accessed 15 Jul 2015].

Hansson, M., L. Andersson, and P. Axe (2011), Areal extent and volume of anoxia and hypoxia in the Baltic Sea, 1960–2011, SMHI Report Series: Report Oceanography, 42. ISSN: 0283-1112.

Hawley, N., T. H. Johengen, Y. R. Rao, S. A. Ruberg, D. Beletsky, S. A. Ludsin, B. J. Eadie, D. J. Schwab, T. E. Croley, and S. B. Brandt (2006), Lake Erie hypoxia prompts Canada-U.S. study, *Eos Trans. AGU*, 87(32), 313–319, doi:10.1029/2006EO320001.

HELCOM (Helsinki Commission) (2007), HELCOM Baltic Sea Action Plan. Baltic Marine Environment Protection Commission (Helsinki Commission), 102 pp. [Available at: <http://www.helcom.fi/baltic-sea-action-plan>; accessed 15 Jun 2015].

This article is protected by copyright. All rights reserved.

Accepted Article

Hipsey, M. R. (2008), The CWR Computational Aquatic Ecosystem Dynamics Model CAEDYM. User Manual. Centre for Water Research, University of Western Australia.

Hodges, B., J. Imberger, A. Saggio, and K. Winters (2000), Modeling basin-scale internal waves in a stratified lake, *Limnol. Oceanogr*., 45, 1603–1620.

Hodges, B., and C. Dallimore (2006), Estuary, lake and coastal ocean model: ELCOM. Science Manual. Centre of Water Research. University of Western Australia.

Howarth, R., F. Chan, D. J. Conley, J. Garnier, S. C. Doney, R. Marino, and G. Billen (2011), Coupled biogeochemical cycles: eutrophication and hypoxia in temperate estuaries and coastal marine ecosystems, *Front*. *Ecol*. *Environ*., 9, 18–26.

Huang, A., Y. R. Rao, Y. Lu, and J. Zhao (2010), Hydrodynamic modeling of Lake Ontario: An intercomparison of three models, *J. Geophys. Res*., 115, C12076, doi:10.1029/2010JC006269.

ICPDR (International Commission for the Protection of the Danube River) (2009), Danube River Basin District Management Plan. International Commission for the Protection of the Danube River. [Available at: <http://www.icpdr.org/icpdr-files/15091>; accessed 15 Jul 2015].

ICPDR (International Commission for the Protection of the Danube River) (2006), Danube Pollution Reduction Programme. International Commission for the Protection of the Danube River. [Available at: <http://www.icpdr.org/icpdr-pages/dprp.htm>; accessed 29 Jun 2015].

Idso, S. B. (1973), On the concept of lake stability, *Limnol*. *Oceanogr*., 18, 681–683.

Idso, S. B., and R. D. Jackson (1969), Thermal radiation from the atmosphere, *J. Geophys. Res*., 74, 5397-5403.IJC (International Joint Commission) (2012), Great Lakes Water Quality Agreement 2012. Protocol Amending the Agreement between Canada and the United States of America on Great Lakes Water Quality; IJC: Windsor, Ontario, Canada, September 7, 2012.

Imberger, J. (1985), The diurnal mixed layer, *Limnol*. *Oceanogr*., 30(4), 737-770.

Kraus, R. T., C. T Knight, T. M. Farmer, A. M. Gorman, P. D. Collingsworth, G. J. Warren,..., and J. D. Conroy (2015), Dynamic hypoxic zones in Lake Erie compress fish habitat, altering

This article is protected by copyright. All rights reserved.

Accepted Article

vulnerability to fishing gears, *Can. J. Fish. Aquat. Sci.*, 72(6), 797-806, doi:10.1139/cjfas-2014-0517.

Leon, L. F., R. E. H. Smith, M. R. Hipsey, S. A. Bocaniov, S. N. Higgins, R. E. Hecky, J. P. Antenucci, J. A. Imberger, and S. J. Guildford (2011), Application of a 3D hydrodynamic-biological model for seasonal and spatial dynamics of water quality and phytoplankton in Lake Erie, *J. Great. Lakes. Res.*, 37, 41–53.

Liu, W., S. A. Bocaniov, K. G. Lamb, and R. E. H. Smith (2014), Three dimensional modeling of the effects of changes in meteorological forcing on the thermal structure of Lake Erie, *J. Great Lakes Res.*, 40, 827–840.

Michalak, A. M., E. J. Anderson, D. Beletsky, S. Boland, N. S. Bosch, T. B. Bridgeman,..., and M. A. Zagorski (2013), Record-setting algal bloom in Lake Erie caused by agricultural and meteorological trends consistent with expected future conditions, *Proc. Natl. Acad. Sci.*, 110(16), 6448-6452.

MR/GOM (Mississippi River/Gulf of Mexico Watershed Nutrient Task Force) (2001), Action plan for reducing, mitigating, and controlling hypoxia in the northern Gulf of Mexico; Office of Wetlands, Oceans, and Watersheds, U.S. Environmental Protection Agency: Washington, DC.

MR/GOM (Mississippi River/Gulf of Mexico Watershed Nutrient Task Force) (2008), Gulf hypoxia action plan, Office of Wetlands, Oceans, and Watersheds, US Environmental Protection Agency, Washington, DC.

Obenour, D. R., A. M. Michalak, and D. Scavia (2015), Assessing biophysical controls on Gulf of Mexico hypoxia through probabilistic modeling, *Ecol. Appl.*, 25(2), 492-505.

Obenour, D., D. Scavia, N. R. Rabalais, E. R. Turner, and A. Michalak (2013), A retrospective analysis of mid-summer hypoxic area and volume in the northern Gulf of Mexico, 1985-2011, *Environ. Sci. Technol.*, 47, 9808− 9815.

Parkinson, C. L., and W. M. Washington (1979), A large-scale numerical model of sea ice, *J. Geophys. Res.*, 84(C1), 311-337.

Rabalais, N. N., R. E. Turner, and W. J. Wiseman Jr. (2002), Gulf of Mexico hypoxia, AKA" The dead zone", *Annu. Rev. Ecol. Syst.*, 33, 235-263.

This article is protected by copyright. All rights reserved.

Accepted Article

Rabalais, N. N., R. E. Turner, B. S. Gupta, D. F. Boesch, P. Chapman, and M. C. Murrell (2007), Hypoxia in the northern Gulf of Mexico: Does the science support the plan to reduce, mitigate, and control hypoxia?, *Estuar. Coast*., 30(5), 753-772.

Rao, Y. R., T. Howell, S. B. Watson, and S. Abernethy (2014), On hypoxia and fish kills along the north shore of Lake Erie, *J. Great Lakes Res*., 40, 187–191.

R Core Team (2014), R: A language and environment for statistical computing. R Foundation for Statistical Computing, Vienna, Austria. [Available at: <http://www.R-project.org/ >; accessed 15 Jun 2015].

Read, J. S., D. P. Hamilton, I. D. Jones, K. Muraoka, L. A. Winslow, R. Kroiss, C. H. Wu, and E. Gaiser (2011), Derivation of lake mixing and stratification indices from high-resolution lake buoy data, *Environ. Modell. Softw*., 26(11), 1325-1336.

Renaud, M. L. (1986), Hypoxia in Louisiana coastal waters during 1983: Implications for fisheries, *Fish. B-NOAA*, 84, 19–26.

Roberts, J. J., T. O. Höök, S. A. Ludsin, S. A. Pothoven, H. A. Vanderploeg, and S. B. Brandt (2009), Effects of hypolimnetic hypoxia on foraging and distributions of Lake Erie yellow perch, *J. Exp. Mar. Biol. Ecol*., 381, S132-S142.

Rodgers, G. K., and D. V. Anderson (1961), A preliminary study of the energy budget of Lake Ontario, *J. Fish. Res. Board Can*., 18(4), 617-636.

Ruberg, S. A., E. Guasp, N. Hawley, R.W. Muzzi, S. B. Brandt, H. A. Vanderploeg,..., and S. A. Constant (2008), Societal benefits of the real-time coastal observation network (ReCON): Implications for municipal drinking water quality, *Mar. Technol. Soc. J*., 42(3), 103-109.

Rucinski, D. K., J. V. DePinto, D. Scavia, and D. Beletsky (2014), Modeling Lake Erie's hypoxia response to nutrient loads and physical variability, *J. Great Lakes Res*., 40, 151–161.

Sambridge, M., J. Braun, and H. McQueen (1995), Geophysical parametrization and interpolation of irregular data using natural neighbours, *Geophys. J. Int*., 122, 837-857.

Scavia, D., J. D. Allan, K. K. Arend, S. Bartell, D. Beletsky, N. S. Bosch,…, and Y. Zhou (2014), Assessing and addressing the re-eutrophication of Lake Erie: central basin hypoxia. *J. Great Lakes Res*., 40(2), 226–246.

This article is protected by copyright. All rights reserved.

Accepted Article

Scavia, D., and J. V. DePinto (2015), Great Lakes Water Quality Agreement Nutrient Annex Objectives and Targets Task Team Ensemble Modeling Report, 229 pp. [Available at: <http://tinyurl.com/ng6d3tn>; accessed 10 Aug 2015].

Schertzer, W. M., J. H Saylor, F. M. Boyce, D. G. Robertson, and F. Rosa (1987), Seasonal thermal cycle of Lake Erie, *J. Great Lakes Res*., 13(4), 468-486.

Schmidt, W. (1928), Über die Temperatur-und Stabilitätsverhältnisse von Seen, *Geograf. Ann*., 10, 145-177.

Schwab, D. J., and J. A. Morton (1984), Estimation of overlake wind speed from overland wind speed: a comparison of three methods, *J. Great Lakes Res*., 10(1), 68-72, doi:10.1016/S0380-1330(84)71808-9.

Sly, L. I., M. C. Hodgkinson, and V. Arunpairojana (1990), Deposition of manganese in a drinking water distribution system, *Appl. Environ. Microb*., 56(3), 628-639.

USEPA (United States Environmental Protection Agency) (2010), Chesapeake Bay total maximum daily load for nitrogen, phosphorus, and sediment. Annapolis, MD: U.S. Environmental Protection Agency, Chesapeake Bay Program Office. [Available at: <http://www.epa.gov/reg3wapd/tmdl/ChesapeakeBay/tmdlexec.html>; accessed 15 Jun 2015].

Väisälä, V. (1925), Über die Wirkung der Windschwankungen auf die Pilotbeobachtungen, *Soc. Sci. Fenn. Commentat. Phys.-Math*., 2(19), 19-37.

Vanderploeg, H. A., S. A. Ludsin, S. A. Ruberg, T. O. Höök, S. A. Pothoven, S. B. Brandt, G. A. Lang, J. R. Liebig, and J. F. Cavaletto (2009), Hypoxia affects spatial distributions and overlap of pelagic fish, zooplankton, and phytoplankton in Lake Erie, *J. Exp. Mar. Biol. Ecol.*, 381, S92-S107.

Vaquer-Sunyer, R., and C. M. Duarte (2008), Thresholds of hypoxia for marine biodiversity, *Proc. Natl. Acad. Sci*., 105(40), 15452-15457.

Zhou, Y., D. R. Obenour, D. Scavia, T. H. Johengen, and A. M. Michalak (2013), Spatial and temporal trends in Lake Erie hypoxia, 1987–2007, *Environ. Sci. Technol*., 47, 899–905, doi:10.1021/es303401b.

This article is protected by copyright. All rights reserved.

Accepted Article

Zhou, Y., D. Scavia, and A. M. Michalak (2014), Nutrient loading and meteorological conditions explain interannual variability of hypoxia in the Chesapeake Bay, *Limnol. Oceanogr*., 59, 373-374, doi:10.4319/lo.2014.59.2.0373.

Zhou, Y., A. M. Michalak, D. Beletsky, Y. R. Rao, and R. P. Richards (2015), Record-breaking Lake Erie hypoxia during 2012 drought, *Environ. Sci. Technol*., 49(2), 800-807, doi:10.1021/es503981n.

Accepted Article

This article is protected by copyright. All rights reserved.

Table 1 The list of index (standard) stations located in the central basin of Lake Erie

Agency	Station name	Latitude	Longitude	Depth (m)
USEPA (GLNPO)	ER30	42.4302	81.2050	19.6
	ER31	42.2535	81.1065	20.7
	ER32	42.0822	81.0118	21.5
	ER36	41.9350	81.4783	22.5
	ER37	42.1112	81.5750	23.5
	ER38	42.2817	81.6713	21.4
	ER42	41.9660	82.0420	21.5
	ER43	41.7892	81.9452	21.5
	ER73	41.9775	81.7570	23.5
	ER78	42.1165	81.2492	21.5
	Average depth:			*21.7*
EC	84	41.9361	81.6456	24.2
	945	42.4003	80.6411	20.6
	946	42.1667	80.6417	23.0
	949	42.2500	81.1081	22.2
	952	42.3583	81.4417	22.3
	953	42.2086	81.4419	23.2
	954	42.0250	81.4417	23.8
	961	41.9078	82.1833	20.5
	962	41.7167	82.1833	19.2
	Average depth:			*22.1*

Abbreviations: USEPA, United States Environmental Protection Agency; GLNPO, Great Lakes National Program Office; EC, Environment Canada.

Accepted Article

This article is protected by copyright. All rights reserved.

Table 2 Discharge and phosphorus load, total (TP) and soluble reactive (SRP), in 2008 for the tributaries included in the model (see also Fig. 1).

#	Tributary	As % of total tributary discharge or nutrient loads in 2008:		
		Discharge	TP	SRP
	West Basin:			
1	Detroit	92.39	23.79	41.1
2	Raisin	0.33	2.50	1.9
3	Maumee	2.33	32.72	22.7
4	Portage	0.19	2.95	6.2
	Central Basin:			
5	Sandusky	0.44	9.8	6.1
6	Huron (Ohio)	0.14	1.7	1.3
7	Vermilion	0.10	1.3	1.3
8	Black	0.14	1.8	0.8
9	Rocky	0.12	1.1	1.1
10	Cuyahoga	0.41	4.1	3.1
11	Chagrin	0.15	1.3	1.9
12	Grand (Ohio)	0.31	1.6	0.6
13	Ashtabula	0.07	0.4	0.2
14	Big Otter	0.12	1.3	1.0
15	Kettle	0.05	0.7	0.8
	East Basin:			
16	Cattaraugus	0.34	2.5	1.2
17	Buffalo	0.38	0.7	0.6
18	Grand (Ontario)	1.16	6.1	5.4
19	Big	0.12	0.9	0.5
Total		*99.28*	*97.2*	*97.8*

Accepted Article

This article is protected by copyright. All rights reserved.

Table 3 Parameters (*a* and *b*) and their 95% confidence intervals (2.5% and 97.5% percentiles) for the predictive equations to estimate the hypoxic extent based on the square of mean bottom DO concentrations at the locations of ten USEPA index stations in central Lake Erie. All equations are in the form of Equation 1 (see text).

Equation #	Hypoxic extent (HE)	Zone	*a*			*b*			*N*	R^2
			Mean	2.5%	97.5%	Mean	2.5%	97.5%		
	For EPA index stations (see Table 1):									
2	HE_1	total	6.04	5.61	6.51	3.28	2.95	3.65	453	0.85
3	HE_2	total	10.63	10.37	10.89	7.00	6.72	7.28	453	0.97
4	HE_3	total	12.92	12.60	13.25	12.25	11.72	12.80	453	0.95
5	HE_4	total	14.18	13.80	14.57	18.32	17.45	19.23	453	0.95
6	HE_1	nearshore	1.93	1.81	2.06	7.12	6.38	7.95	447	0.79
7	HE_2	nearshore	4.07	3.90	4.26	11.20	10.36	12.12	453	0.86
8	HE_3	nearshore	5.72	5.50	5.94	16.26	15.17	17.42	453	0.87
9	HE_4	nearshore	6.87	6.63	7.11	22.22	20.83	23.64	453	0.87
10	HE_1	offshore	4.83	4.38	5.32	2.09	1.87	2.34	447	0.76
11	HE_2	offshore	7.17	6.98	7.36	4.61	4.43	4.79	453	0.97
12	HE_3	offshore	7.46	7.27	7.65	9.24	8.87	9.64	453	0.95
13	HE_4	offshore	7.49	7.29	7.68	15.15	14.47	15.85	453	0.94
	For EC index stations (see Table 1):									
14	HE_1	total	5.93	5.51	6.39	3.45	3.11	3.84	447	0.83
15	HE_2	total	11.49	11.21	11.78	6.06	5.84	6.30	453	0.97
16	HE_3	total	13.47	13.16	13.78	10.89	10.46	11.34	453	0.97
17	HE_4	total	14.59	14.24	14.93	16.93	16.21	17.67	453	0.95
18	HE_1	nearshore	2.16	2.03	2.31	5.83	5.30	6.44	447	0.83
19	HE_2	nearshore	4.43	4.25	4.61	9.35	8.72	10.02	453	0.90
20	HE_3	nearshore	5.98	5.77	6.19	14.37	13.48	15.29	453	0.90
21	HE_4	nearshore	7.04	6.82	7.26	20.41	19.23	21.60	453	0.90
22	HE_1	offshore	4.85	4.39	5.35	2.21	1.98	2.46	447	0.75
23	HE_2	offshore	7.53	7.22	7.85	4.28	4.06	4.52	453	0.92
24	HE_3	offshore	7.66	7.43	7.89	8.44	8.04	8.86	453	0.94
25	HE_4	offshore	7.66	7.47	7.85	13.91	13.32	14.51	453	0.95

Abbreviations: R^2, coefficient of determination; *N*, the number of observations.

Accepted Article

This article is protected by copyright. All rights reserved.

Table 4 Mean and 95% confidence intervals (2.5% and 97.5% percentiles) in brackets of estimated hypoxic extent based on bottom measurements of DO at ten index stations in the central Lake Erie from summer GLNPO cruises for 2000 – 2014 using formulas derived from three-dimensional hydrodynamic and water quality model of Lake Erie (see Table 3).

Year	Month	Date	Hypoxic Extent (HE; 10^3 km^2)			
			HE_1	HE_2	HE_3	HE_4
2000	8	3-4	2.50 (*2.32 – 2.95*)	7.03 (*6.86 - 7.32*)	10.33 (*10.09 – 10.68*)	12.11 (*11.79 – 12.54*)
2001	8	5-6	0.62 (*0.58 – 0.84*)	3.66 (*3.57 – 3.91*)	6.80 (*6.64 – 7.14*)	9.44 (*9.19 – 9.89*)
2002	8	6-7	0.03 (*0.03 – 0.05*)	0.88 (*0.85 – 0.99*)	2.71 (*2.65 – 2.95*)	5.46 *(5.32 – 5.87)*
2003	8	8	0.15 (*0.14 – 0.24*)	1.90 (*1.86 – 2.08*)	4.46 (*4.36 – 4.76*)	7.35 (*7.15 – 7.79*)
2004	8	6	*No Anoxia*	0.36 (*0.35 – 0.43*)	1.54 (*1.51 – 1.71*)	3.90 (*3.80 – 4.27*)
2005	8	9-10	0.02 (*0.02 – 0.04*)	0.72 (*0.70 – 0.82*)	2.39 (*2.34 – 2.62*)	5.07 (*4.93 – 5.47*)
2006	8	10-12	0.51 (*0.47 – 0.70*)	3.33 (*3.25 – 3.57*)	6.39 (*6.24 – 6.73*)	9.10 (*8.86 – 9.55*)
2007	8	8	0.09 (*0.09 – 0.16*)	1.52 (*1.40 – 1.68*)	3.86 (*3.77 – 4.15*)	6.74 (*6.56 – 7.18*)
2008	8	9-10	0.03 (*0.03 – 0.06*)	0.93 (*0.91 – 1.05*)	2.81 (*2.75 – 3.06*)	5.59 (*5.44 – 6.00*)
2009	8	18-19	*No Data*	*No Data*	*No Data*	*No Data*
2010	8	9-10	0.46 (*0.43 – 0.65*)	3.20 (*3.12 – 3.43*)	6.22 (*6.08 – 6.56*)	8.96 (*8.72 – 9.41*)
2011	8	10	0.02 (*0.02 – 0.04*)	0.77 (*0.75 – 0.87*)	2.49 (*2.43 – 2.72*)	5.19 (*5.05 – 5.60*)
2012	8	10	3.21 (*2.98 – 3.69*)	7.90 (*7.71 – 8.19*)	11.14 (*10.88 – 11.48*)	12.66 (*12.32 – 13.08*)
2013	8	10	2.45 (*2.27 – 2.89*)	6.97 (*6.79 – 7.25*)	10.27 (*10.03 – 10.62*)	12.06 (*11.74 – 12.49*)
2014	8	14-15	*No Anoxia*	0.02 (*0.02 – 0.03*)	0.25 (*0.25 – 0.30*)	1.33 (*1.30 – 1.53*)

This article is protected by copyright. All rights reserved.

Figures legends

Figure 1. Map of Lake Erie with the locations of the USEPA stations and all included inflows and outflow (indicated by an arrow with the name of the corresponding river). Dotted lines represent 10-m contours.

Figure 2. Time-series of the observed and simulated daily lake-wide surface temperatures (a); plots of the observed vs simulated values of daily lake-wide temperatures (b), temperatures averaged over the top six meters of the surface mixed layer (c), and bottom temperatures (d).

Figure 3. Comparison of the observed (open circles) and simulated (solid line) water column profiles at stations ER31 (a-g; o-p) and ER78 (h-n; q-r) for temperature (a-g; h-n) and dissolved oxygen (o-p; q-r).

Figure 4. Observed (solid circles) and simulated (solid line) bottom dissolved oxygen (DO) at stations ER32 (a), ER37 (b), ER38 (c), and ER42 (d). Simulated vs observed bottom DO for the seven USEPA cruises in 2008 (e).

Figure 5. Plot of daily hypoxic extents HE_2 simulated by the 3D model and those predicted from the Zhou model vs the average simulated daily bottom DO at ten USEPA index stations in central Lake Erie (DO_m) for 2008 for the period from April 21 to October 30 (a), from April 21 to September 15 (b), and from September 16 to October 28 (c). The thin arrows on panel (c) show the progression of time, while the thicker arrows with the label "winds" indicate the times of the occurrences of the strong wind events (see also Fig. S2 in SI for the strong wind events). Time series plots of HE_2 of the simulated results with 3D model (thick solid line) and predicted by the Zhou model based on the average simulated daily bottom DO at ten USEPA index stations (thin solid line) and field observations (open circles).

This article is protected by copyright. All rights reserved.

Figure 6. (a) Comparison of the hypoxic extents HE_2 in the central basin between those predicted by Equation 3 (Table 3) from the field bottom DO observations and those reported in Zhou et al. (2013, 2015) for the late summer (August) GLNPO cruises from 2000 to 2012 inclusive including the data shown in right panel. Horizontal thin solid lines indicate the 95% confidence intervals in Zhou's et al. (2013, 2015) results. (b) Hypoxic extents HE_2 for some selected years, 2003, 2005 and 2012, with the following dates: August 8 and 19-20 (a1, a2), September 2-3 and 15-16 (a3, a4); August 6 and September 15-16 (a5, a6); August 10-11, 30-31 and September 10-11 (a7, a8, a9). The median values from Zhou et al. (2013, 2015) are shown by the open circles; while open triangles indicate the mean values calculated using Equation 3 (Table 3) from the field bottom DO observations. Vertical thin solid lines indicate the 95% confidence intervals (2.5% and 97.5% percentiles).

Figure 7. Plot of daily (anoxic) extent HE_1 vs average simulated daily bottom DO at ten USEPA index stations in the central Lake Erie (DO_m) for the entire simulation period in 2008 (a) and for the period from April 21 to September 13, 2008 (b). Plot of anoxic extents HE_1 predicted by equation for HE_1 shown in sub-panel b and based on simulated DO_m and hypoxic extents HE_2 predicted by Zhou model (Zhou at al., 2013) for the same DO_m (c). Plot of anoxic extents HE_1 simulated by 3D model vs those HE_1 predicted by Zhou model and based on simulated DO_m (d).

Figure 8. Estimated historical areal extents of central basin hypoxia for different threshold concentrations of DO <1 (HE_1; a), < 2 (HE_2; b), < 3 (HE_3; c) and 4 mg L^{-1} (HE_4; d) for the past fifteen years (2000 to 2014) based on the equations derived in this study (Eqs. 2 to 5, Table 3) and observed DO concentrations during summer cruises (GLENDA data).

This article is protected by copyright. All rights reserved.

Figure 9. Simulated seasonal dynamics of HE_1 (a, c, e) and HE_2 (b, d, f) for basin-wide, nearshore and offshore zones in 2008 ('normal' year; a-b) and using meteorological conditions for 1996 (c-d) and 2012 (e-f) accounting for the meteorological conditions of the 'cool' and 'warm' years, respectively. The vertical light and dark grey bars indicate timing in days (mean ±SD) of all central basin DO monitoring cruises from 1987 to 2007 for all agencies (CLNPO, GLERL and NWRI; $N = 75$) and some selected agencies (GLNPO and GLERL; $N = 26$), respectively, based on data provided in Table S1 in Zhou et al. (2013).

Figure 10. Simulated seasonal dynamics of the whole basin hypoxic extents HE_1, HE_2, HE_3 and HE_4 for 'normal' year (a), 'cool' year (b) and 'warm' year (c). See the legend of Fig. 9 for the meanings of the vertical light and dark grey bars.

Accepted Article

This article is protected by copyright. All rights reserved.

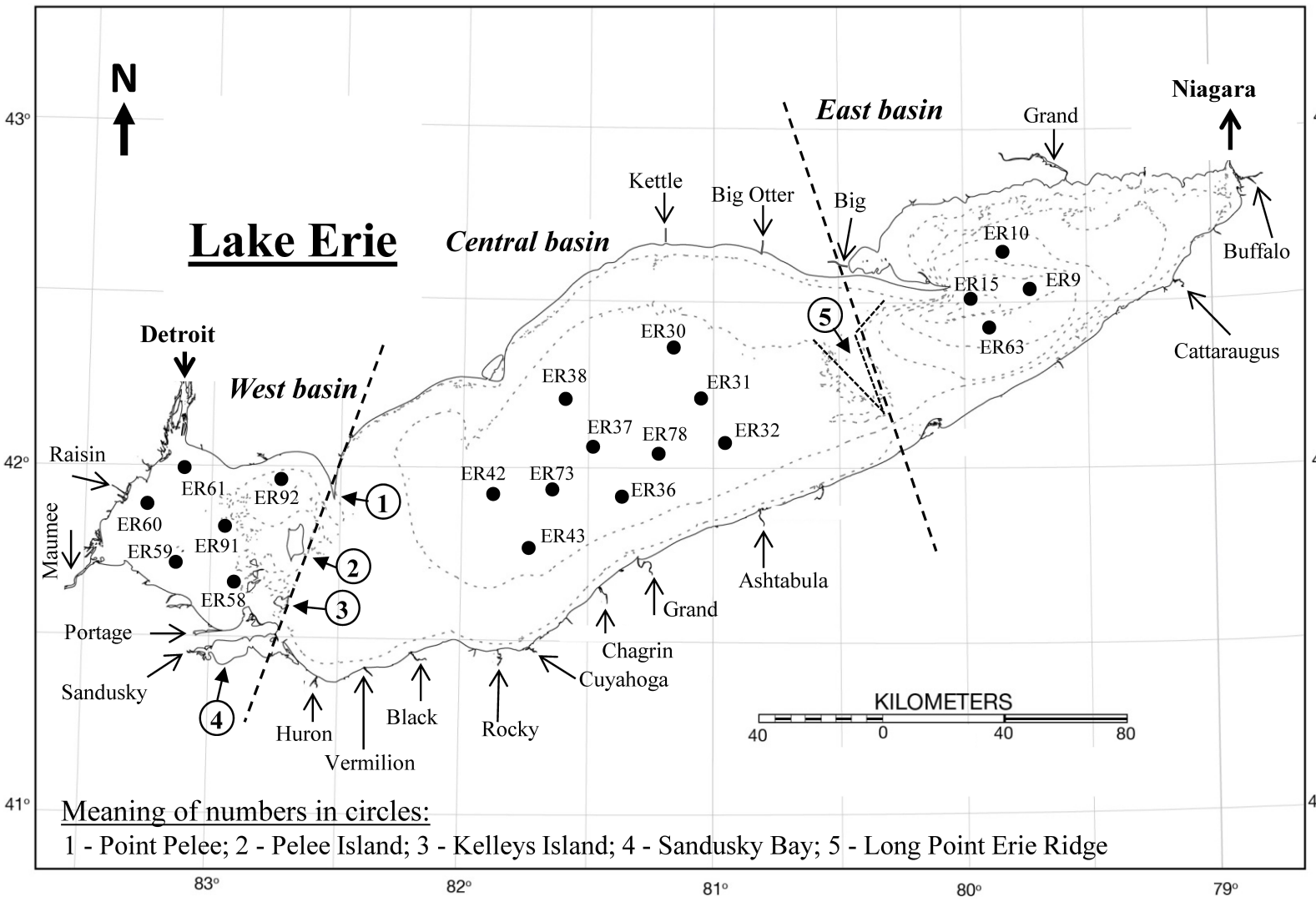

Meaning of numbers in circles:

1 - Point Pelee; 2 - Pelee Island; 3 - Kelleys Island; 4 - Sandusky Bay; 5 - Long Point Erie Ridge

This article is protected by copyright. All rights reserved.

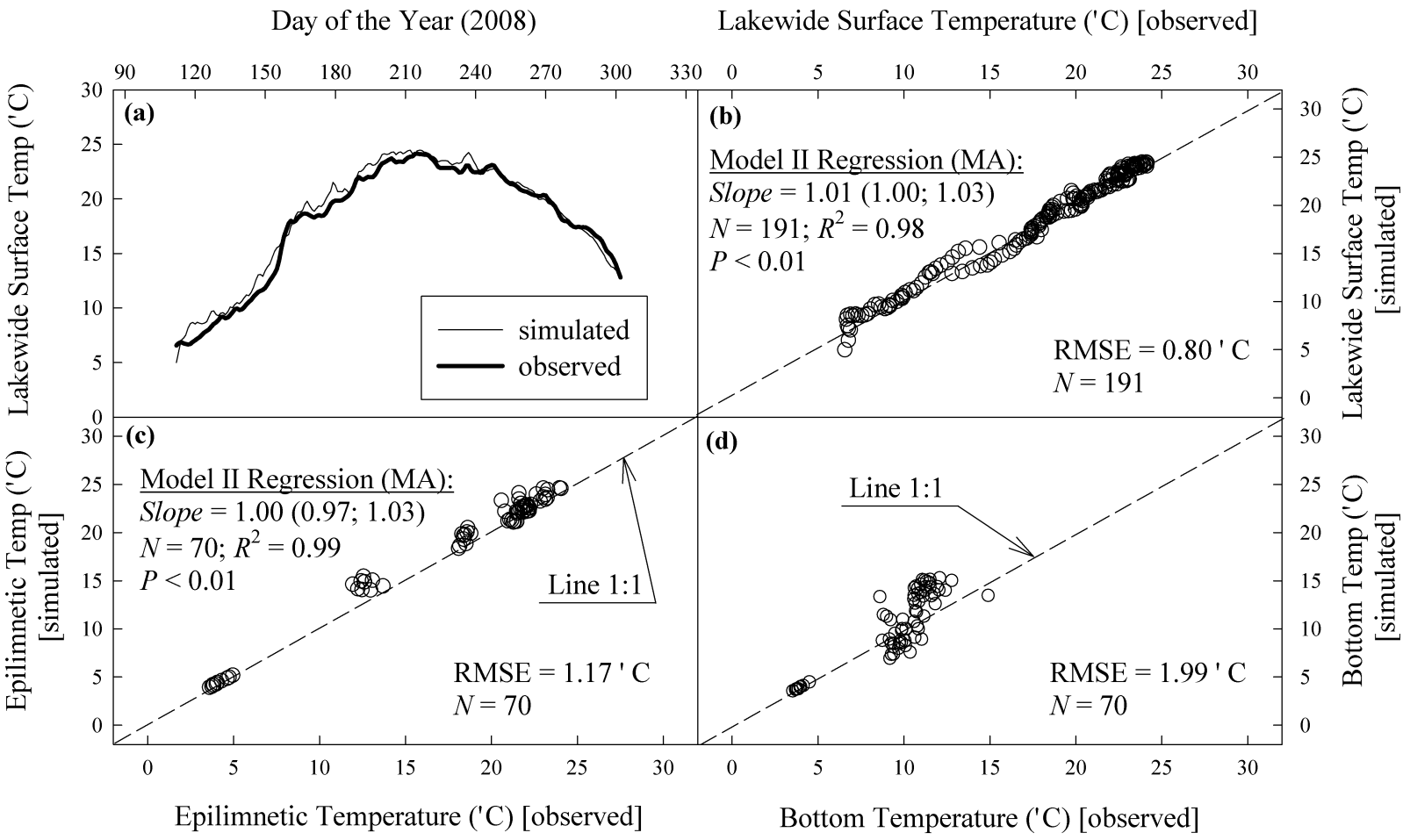

This article is protected by copyright. All rights reserved.

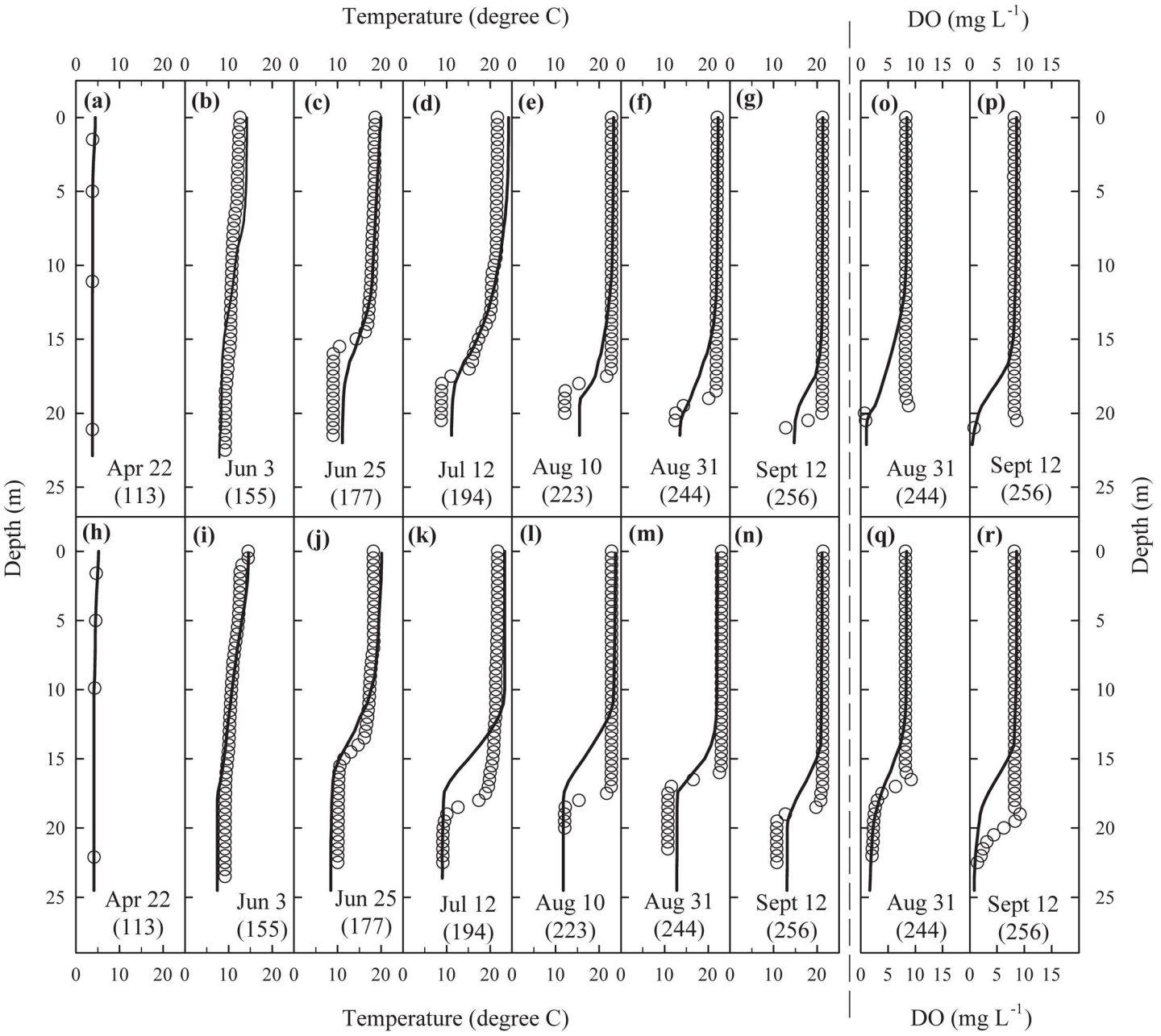

This article is protected by copyright. All rights reserved.

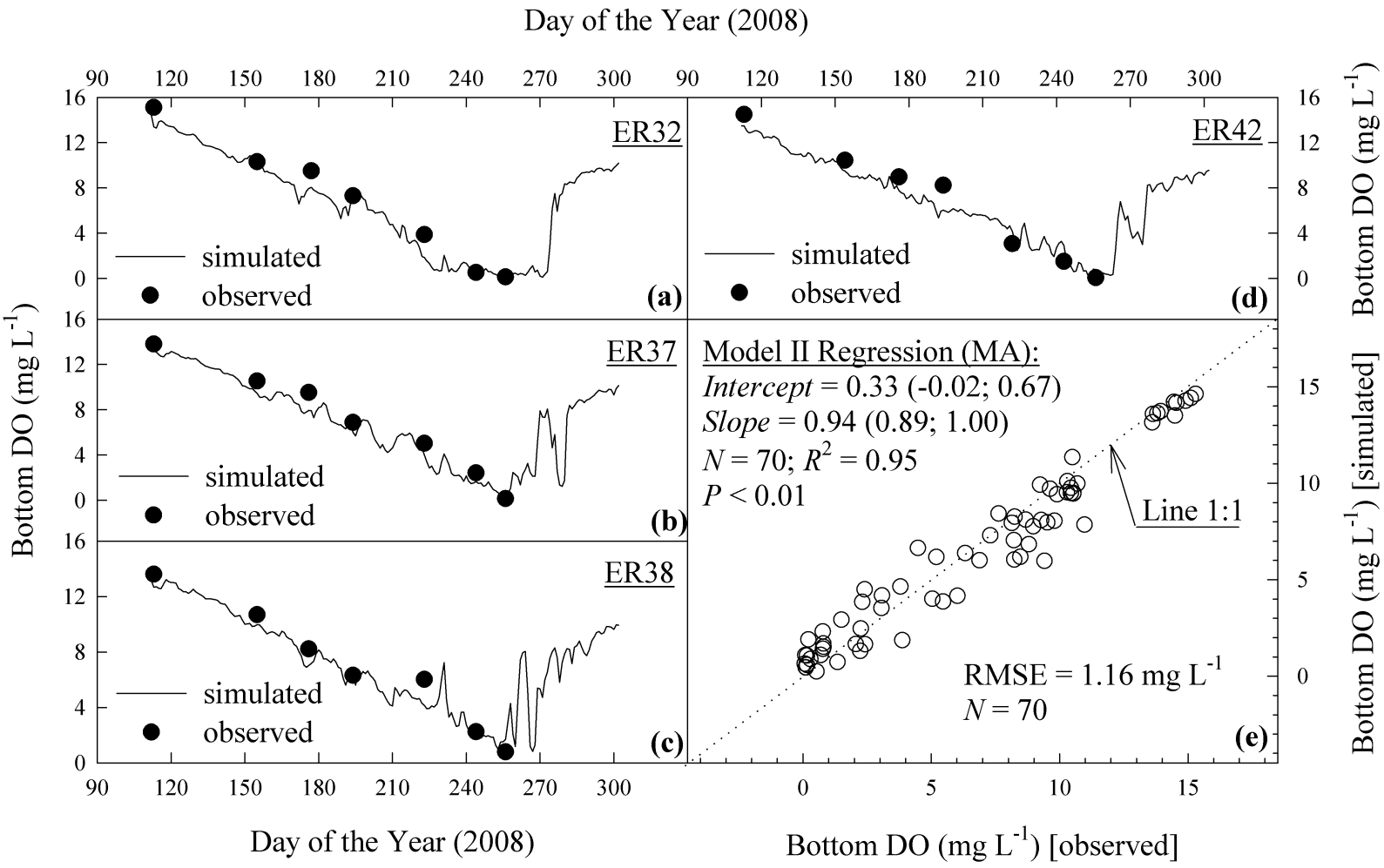

This article is protected by copyright. All rights reserved.

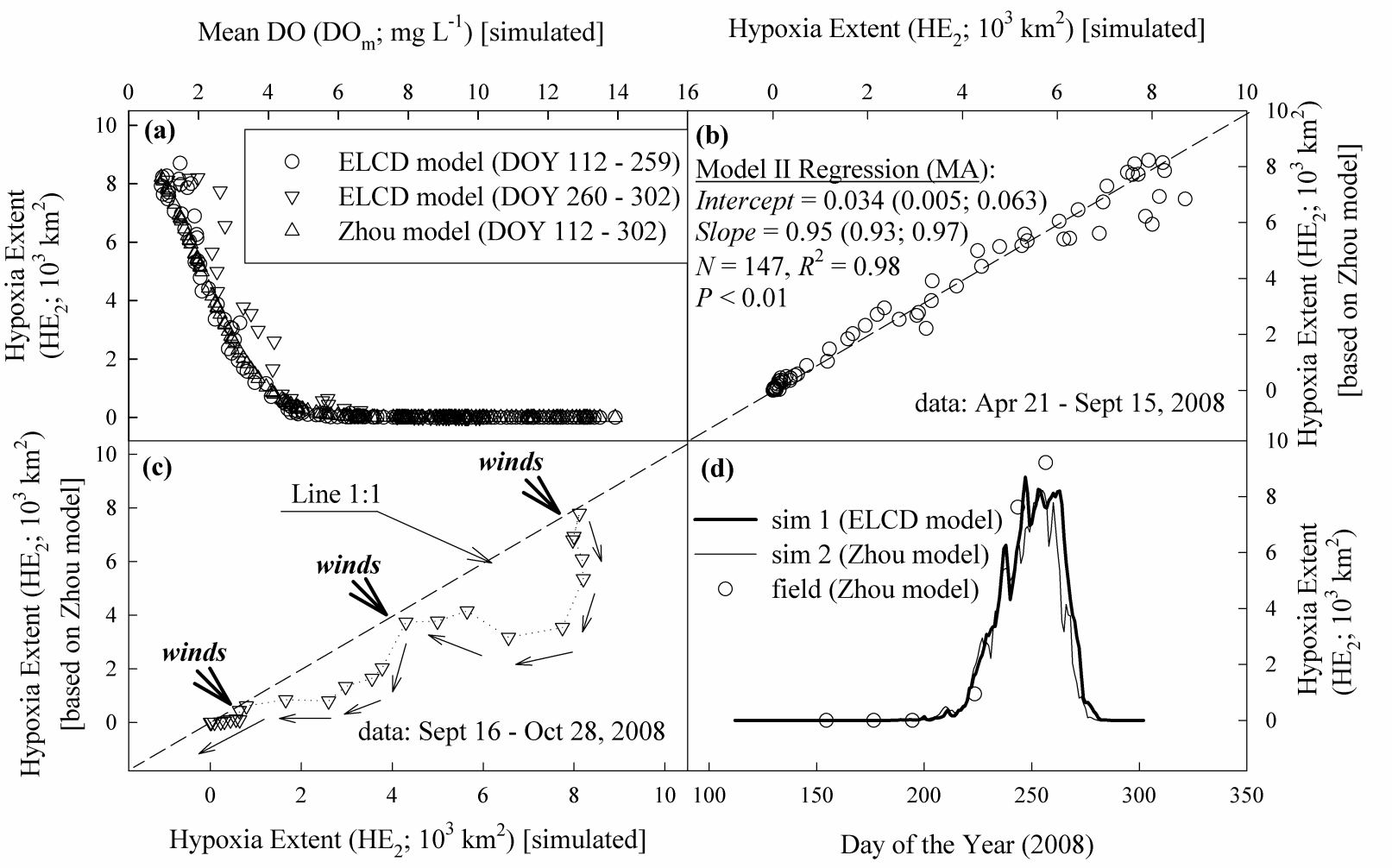

This article is protected by copyright. All rights reserved.

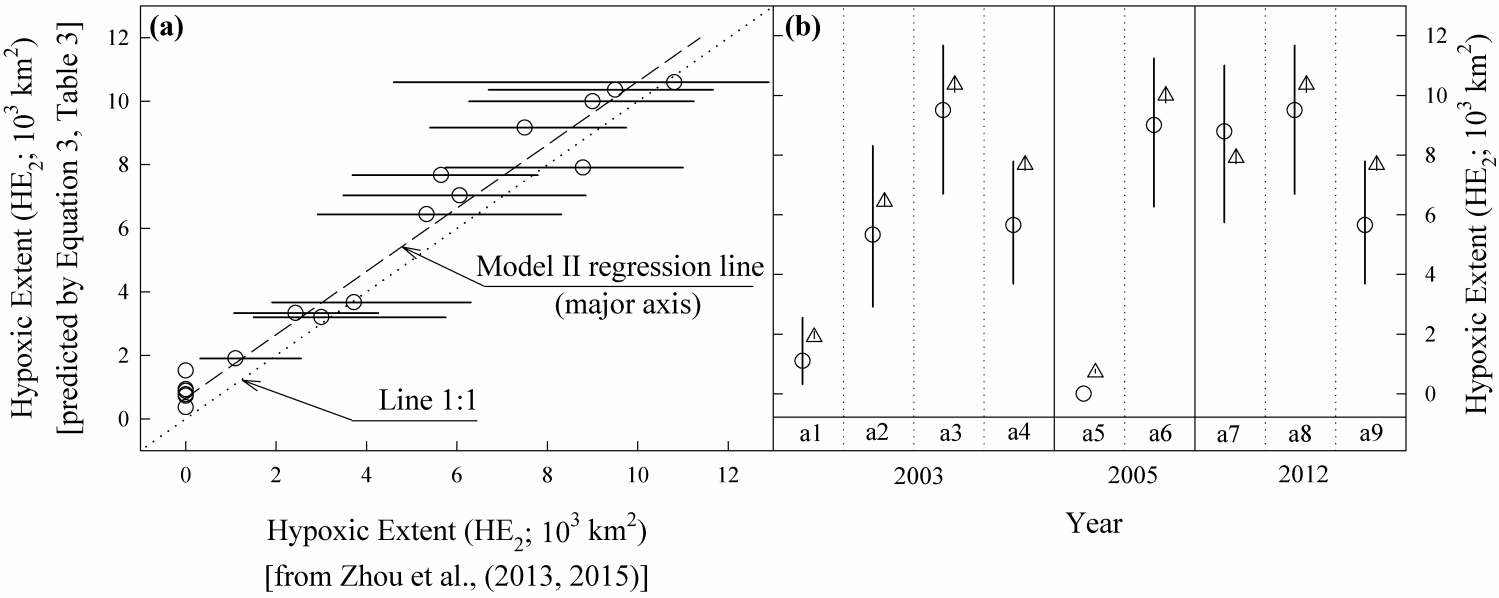

This article is protected by copyright. All rights reserved.

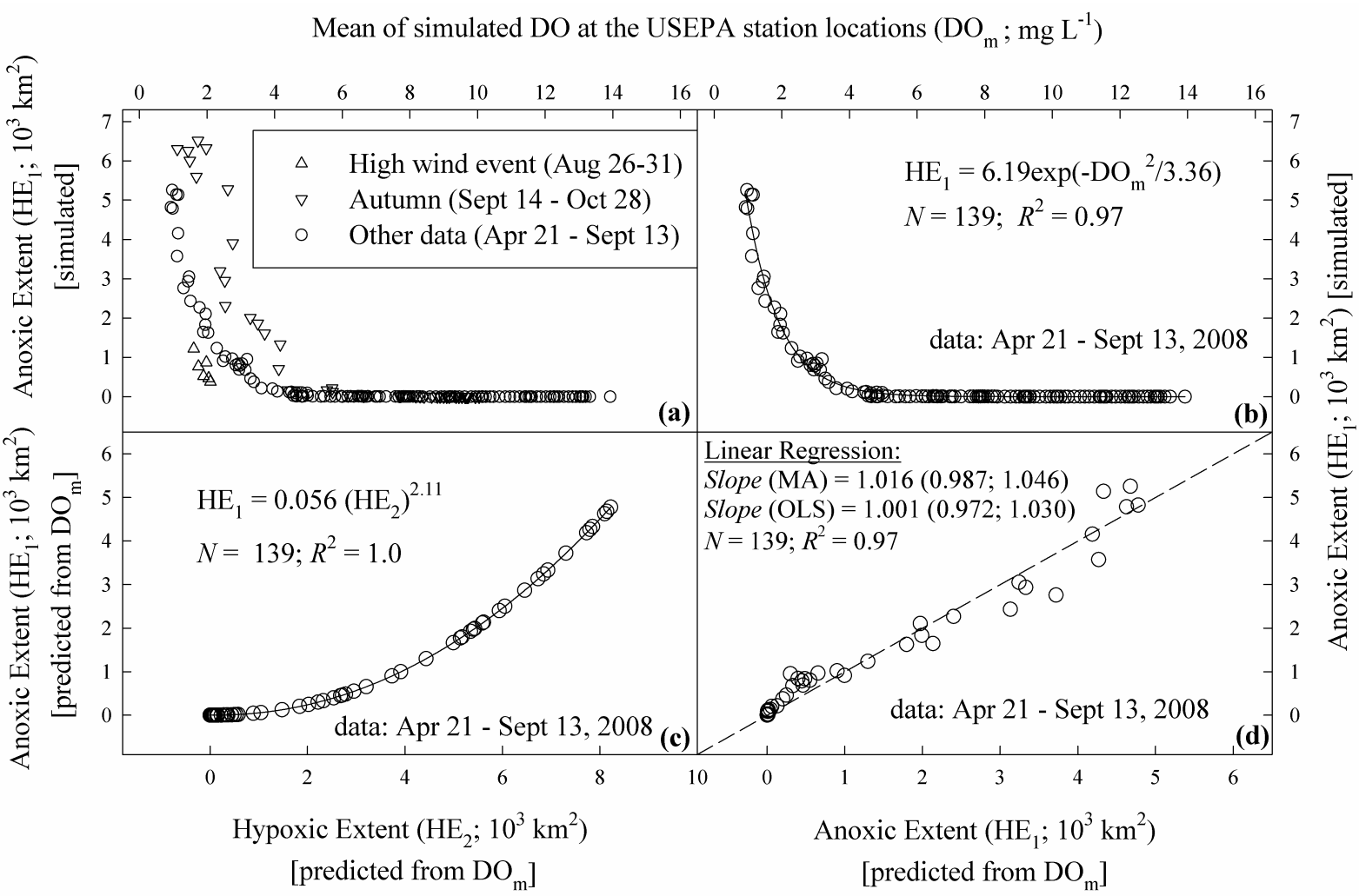

This article is protected by copyright. All rights reserved.

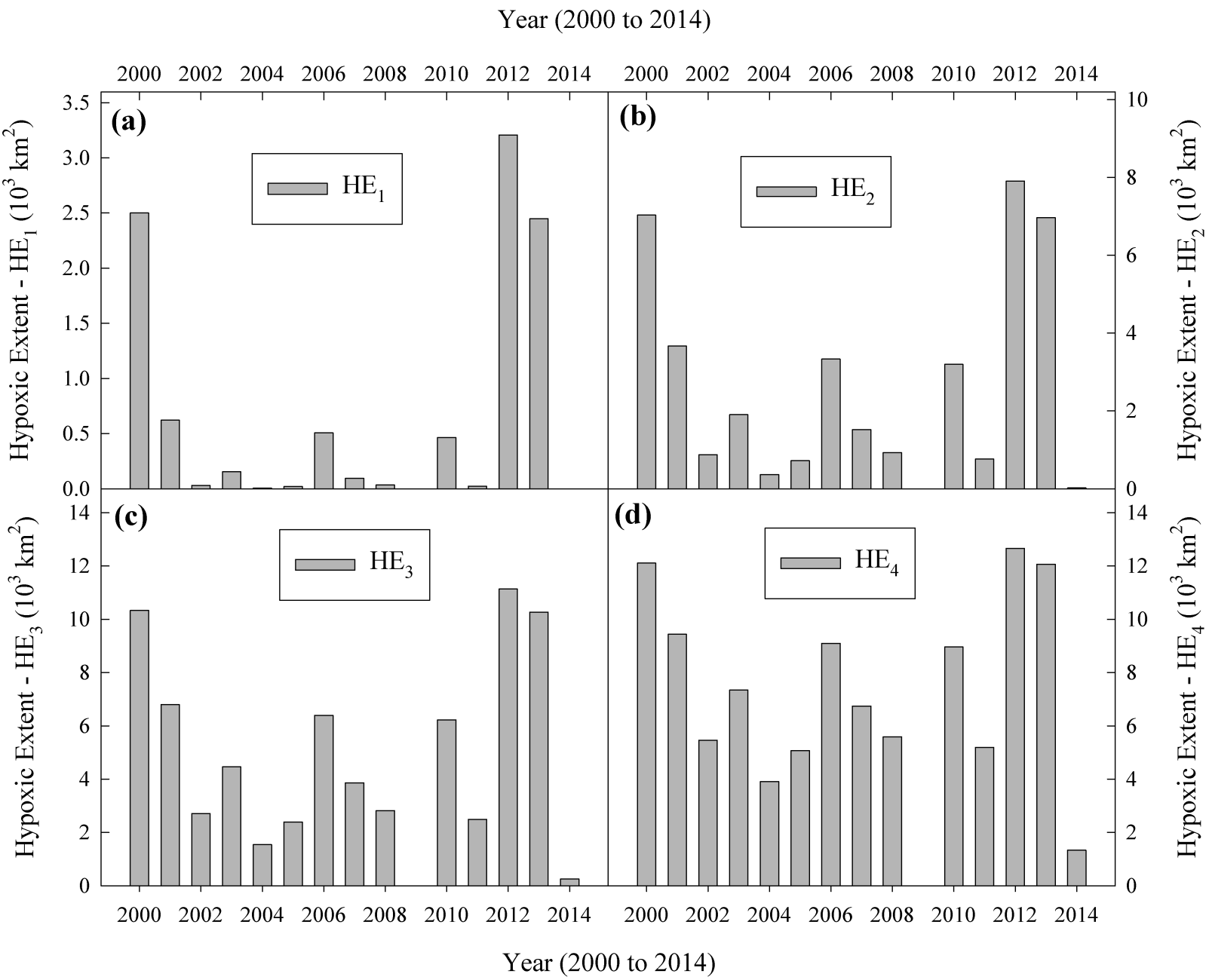

This article is protected by copyright. All rights reserved.

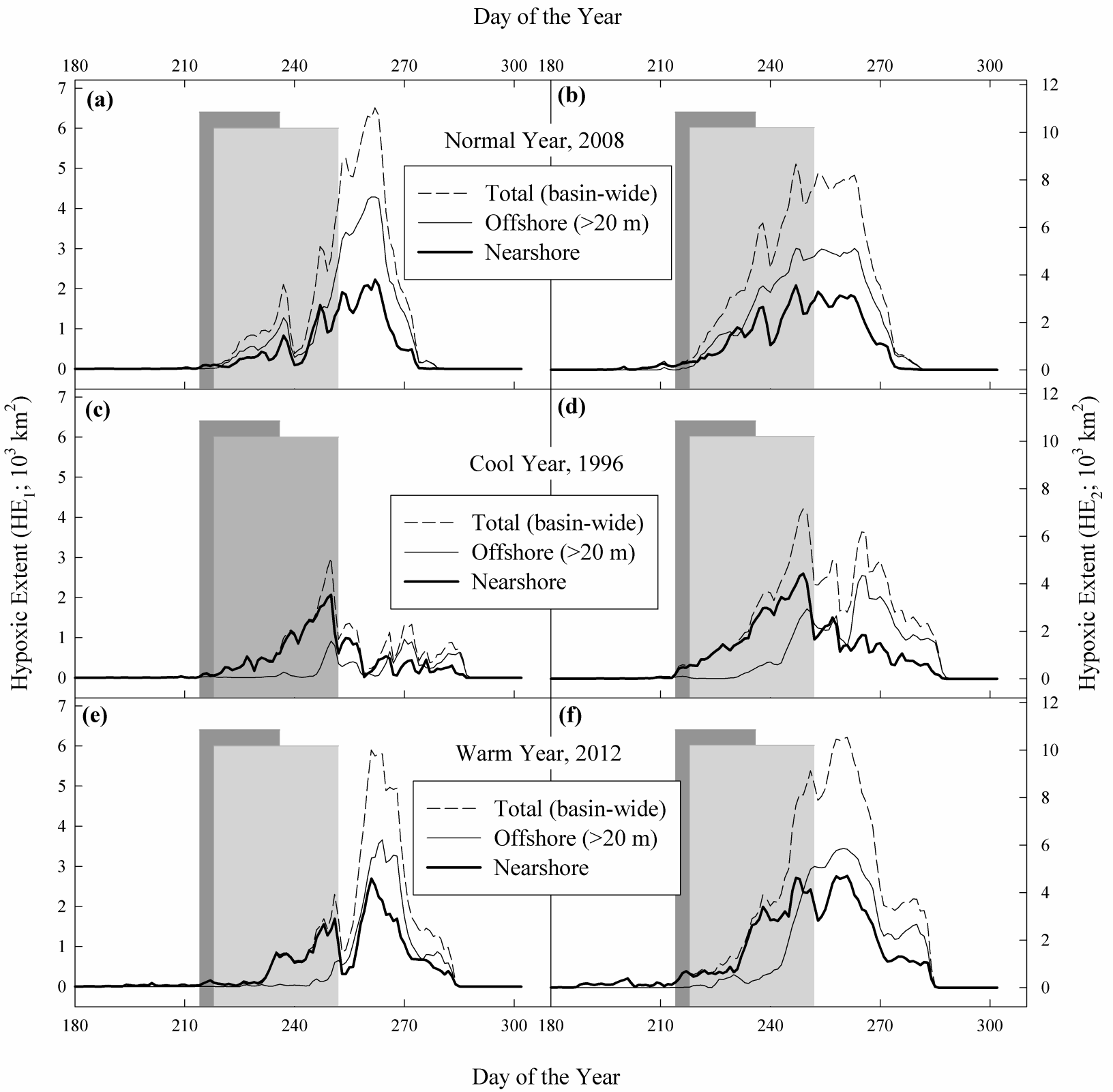

This article is protected by copyright. All rights reserved.

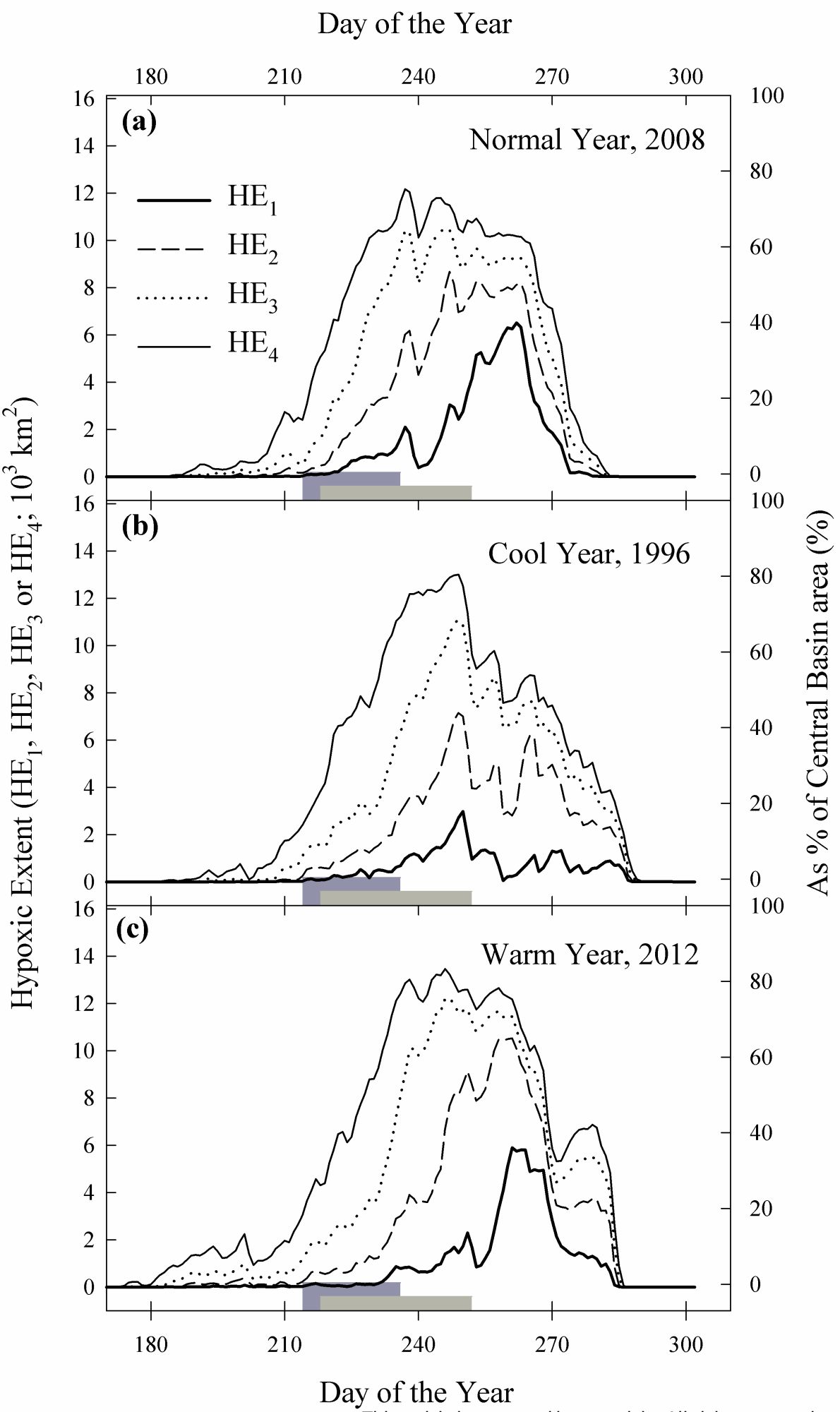

This article is protected by copyright. All rights reserved.